Biomaterials 33 (2012) 7794–7802

Contents lists available at SciVerse ScienceDirect

Biomaterials

journal homepage: www.elsevier.com/locate/biomaterials

The long-term stability and biocompatibility of fluorescent nanodiamond as an *in vivo* contrast agent

V. Vaijayanthimala [a,1], Po-Yun Cheng [b,1], Shih-Hua Yeh [c], Kuang-Kai Liu [b], Cheng-Hsiang Hsiao [d,e,**], Jui-I Chao [b,***], Huan-Cheng Chang [a,c,*]

[a] *Institute of Atomic and Molecular Sciences, Academia Sinica, Taipei 10672, Taiwan, ROC*
[b] *Department of Biological Science and Technology, National Chiao Tung University, Hsinchu 30068, Taiwan, ROC*
[c] *Department of Chemistry, National Taiwan University, Taipei 10672, Taiwan, ROC*
[d] *Department of Pathology, National Taiwan University Hospital, Taipei 10002, Taiwan, ROC*
[e] *General Education Center, National Taipei University of Nursing and Health Sciences, Taipei 11219, Taiwan, ROC*

ARTICLE INFO

Article history:
Received 18 April 2012
Accepted 28 June 2012
Available online 3 August 2012

Keywords:
Animal model
Biocompatibility
Diamond
Fluorescence
Nanoparticle
Sentinel lymph node

ABSTRACT

Nanocarbon is a promising type of biomaterial for diagnostic and therapeutic applications. Fluorescent nanodiamond (FND) containing nitrogen-vacancy centers as built-in fluorophores is a new addition to the nanocarbon family. Here, we study the long-term stability and biocompatibility of 100-nm FNDs in rats through intraperitoneal injection over 5 months and develop the potential application of this biomaterial for sentinel lymph node mapping in a mouse model. From both *in vivo* and *ex vivo* fluorescence imaging as well as transmission electron microscopy, we found that the intradermally administered FND particles can be drained from the injection sites by macrophages and selectively accumulated in the axillary lymph nodes of the treated mice. Our measurements of water consumption, fodder consumption, body weight, and organ index showed no significant difference between control and FND-treated groups of the rats. Histopathological analysis of various tissues and organs indicated that FNDs are non-toxic even when a large quantity, up to 75 mg/kg body weight, of the particles was administered intraperitoneally to the living animals. With the properties of wide-ranging biocompatibility and perfect chemical and photophysical stability, FND is well suited for use as a contrast agent for long-term *in vivo* imaging.

1. Introduction

The application of nanotechnology to cancer therapy and drug delivery is a topic of current interest in nanomedicine [1–3]. It has opened up many exciting new opportunities for diagnosing, treating, and tracking the progress of cancer development in molecular and cellular detail. Nanodiamond (ND) has recently emerged as a promising biomaterial for such applications [4–6]. The material can be produced by either detonation, high-pressure-high-temperature (HPHT), or chemical vapor deposition (CVD) methods, followed by deagglomeration or milling processes [7]. Several biocompatibility studies of the particles *in vitro* with various cell lines have shown that ND is among the least toxic of all carbon-based nanomaterials tested so far [8,9]. Moreover, NDs after internalization do not cause any obvious cytotoxic or detrimental effects on the proliferation and differentiation of cells [10,11]. The chemical and biological inertness, augmented by the fact that diamond can be emit far-red fluorescence from a variety of optically active defects [12], is a definite advantage when using NDs for *in vivo* applications.

In the past few years, there have been some studies on the biocompatibility and biodistribution of NDs *in vivo*. Specifically, Puzyr et al. [13] investigated the biocompatibility of detonation nanodiamonds (DNDs) injected subcutaneously into mice and found no inflammatory response at 3 months post-dosing. However, intravenous administration of DNDs into rabbits could change the values of some blood biochemical parameters such as the total bilirubin concentration. Yuan et al. [14,15] have recently studied the *in vivo* biodistribution and dose-dependent liver and hematological toxicity of NDs in mice. Intratracheal instillation of 4-nm DNDs and 50-nm HPHT-NDs did not show any significant

* Corresponding author. Institute of Atomic and Molecular Sciences, Academia Sinica, Taipei 10672, Taiwan, ROC. Tel.: +886 2 23668260; fax: +886 2 2362 0200.
** Corresponding author. Department of Pathology, National Taiwan University Hospital, Taipei 10002, Taiwan, ROC. Tel.: +886 2 23123456xt65457; fax: +886 2 23934172.
*** Corresponding author. Tel.: +886 3 5712121; fax: +886 3 5556219.
E-mail addresses: chhsiao7@ntu.edu.tw (C.-H. Hsiao), jichao@faculty.nctu.edu.tw (J.-I. Chao), hchang@gate.sinica.edu.tw (H.-C. Chang).
[1] These two authors contribute equally to this work.

0142-9612/$ – see front matter © 2012 Elsevier Ltd. All rights reserved.
http://dx.doi.org/10.1016/j.biomaterials.2012.06.084

pulmonary toxicity and no evidence on lipid peroxidation of the lung was detected. Marcon et al. [16] have further assessed the *in vitro* and *in vivo* toxicity of DNDs with different surface modifications (−OH, $-NH_2$, or $-CO_2H$) in HEK 293 cells and *Xenopus laevis*. Cell viability assays revealed that NDs were not toxic to HEK 293 cells at concentrations less than 50 μg/mL, whereas microinjection of ND-CO_2H into early-stage *X. laevis* embryos caused embryotoxicity and teratogenicity. Most recently, Rojas et al. [17] studied the *in vivo* biodistribution of DNDs labeled with ^{18}F in rats by using positron emission tomography and evaluated the impact of kinetic particle size on biodistribution. Their results showed that the radio-labeled DNDs largely accumulated in the lung, spleen, and liver, and also excreted into the urinary tract. Removal of larger particles by prior filtration effectively prevented the particle accumulation in lung and spleen.

We present herein the result of our study on the long-term stability and biocompatibility of fluorescent nanodiamonds (FNDs) in a rat model through intraperitoneal injection over a time period of 5 months. It is an extension of our previous studies of FNDs in *Caenorhabditis elegans* [18] and zebrafish (*Danio rerio*) [19], where we showed that the carbon-based nanomaterial does not induce any detectable oxidative stress response at the whole organism level. In this study, after confirming the non-toxic nature of the nanomaterial in rats, we apply the FND particles for sentinel lymph node mapping by both *in vivo* and *ex vivo* imaging in mice. Sentinel lymph node (SLN) mapping is an important step in SLN biopsy, by which doctors can determine the cancer stage and accounts for the choice of therapy [20]. Although near-infrared quantum dots (QDs) have been successfully applied for the purpose [21], the notion of using potentially toxic, heavy-metal-based QDs for SLN mapping in humans is still under serious debate [1,22]. The non-toxic FNDs clearly offer a favorable alternative and, to the best of our knowledge, no such applications have been reported so far.

The FNDs used in this work were produced by ion irradiation and subsequent annealing of synthetic type Ib ND powders [23–25]. These particles contain negatively charged nitrogen-vacancy (NV^-) defect centers (with a concentration of up to 10 ppm [25]) as built-in fluorophores. Excitation of the NV^- with green yellow light yields exceptionally stable photoluminescence with a zero-phonon line at 638 nm, accompanied with a broad phonon sideband spanning from 600 to 800 nm [26]. Nearly 70% of the fluorescence lies in the near-infrared window (Fig. 1a) [27], making it suitable for optical bioimaging applications [28]. Aside from this potential usefulness, the fluorescence lifetime ($\tau = 11.6$ ns in bulk diamond [29]) of the NV^- center is substantially longer than that (typically $\tau < 4$ ns) of cell and tissue autofluorescence [30], which allows for the utilization of various time-gating techniques to enhance the image contrast [31,32]. Further improvement of the contrast is possible by taking advantages of the spin properties of the NV^- center, which is magneto-optical and can be magnetically manipulated [33].

Three injection methods were employed in this study: intradermal (i.d.), intraperitoneal (i.p.), and subcutaneous (s.c.) administrations. We first conducted s.c. injection of FND solution into rat skin to investigate the long-term stability of the nanomaterial *in vivo* for more than 1 month. We then performed i.d. injection of the FND solution into mouse paws for SLN imaging and short-term toxicity assessment. With i.p., we were able to inject a relatively large amount (up to 23 mg per rat) of FNDs into the intraperitoneal

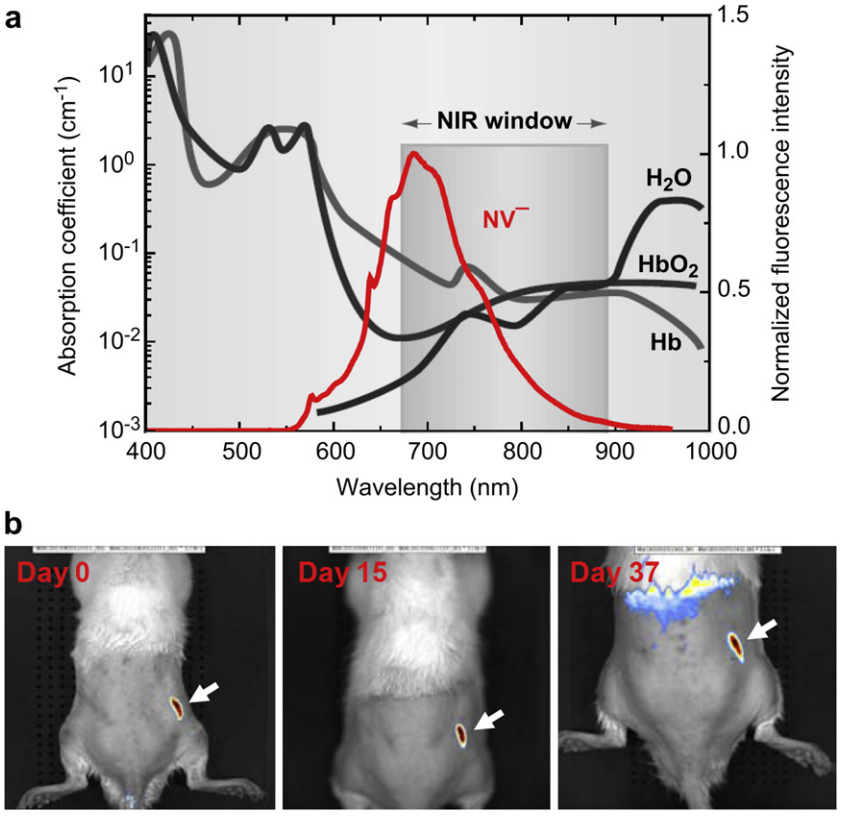

Fig. 1. (a) Comparison of the fluorescence spectrum (red curve) of NV^- centers in FNDs with the near-infrared (NIR) window of biological tissues. The black, dark gray, and light gray curves are the absorption spectra of H_2O, oxygen-bound hemoglobin (HbO_2), and hemoglobin (Hb), respectively. The absorption spectra were adapted from Ref. [27]. (b) Long-term stability test of FNDs in a rat after s.c. injection. Images of the same rat were acquired over a time period of more than 37 days. White arrows indicate the site of FND injection. (For interpretation of the references to color in this figure legend, the reader is referred to the web version of this article.)

cavities of the rats to address its long-term biocompatibility at high doses. Finally, we carried out detailed histopathological analysis of rat tissues to reveal whether the injected FND particles would cause any inflammation or general toxicity in this animal model. Important implications of these results are discussed.

2. Materials and methods

2.1. Production of FNDs

Synthetic type Ib diamond powders (Micron + MDA 0-0.10, Element Six) were radiation-damaged by using either a 40-keV He^+ beam at a dose of $\sim 1 \times 10^{14}$ ions/cm^2 or a 3-MeV H^+ beam at a dose of $\sim 1 \times 10^{16}$ ions/cm^2 to create the optimum amount of vacancies in the diamond crystal lattice, as previously described [25]. They were subsequently annealed in vacuum at 800 °C for 2 h to form FNDs. After being oxidized in air at 450 °C for 1 h and washed in concentrated sulfuric and nitric acid (3:1, v/v) solution at 100 °C for 3 h [11], the NV^--containing particles were extensively rinsed in distilled deionized water (DDW) and stored at room temperature prior to use. A comprehensive characterization of the FNDs prior to bioconjugation and injection can be found in [23,24,34] and also in Figures S1 and S2 of Supporting Information.

2.2. Preparation of BSA-coated FNDs

Acid-washed FNDs were sonicated in DDW for 30 min and then mixed with bovine serum albumin (BSA) in the weight ratio of 1:2 [34]. After vortex mixing for 1 h, excess BSA was removed by DDW wash once, followed by five washes with phosphate-buffered saline (PBS) using centrifugal filter devices (Amicon Ultra-15, 100 K or Amicon Ultra-4, 3 K, Millipore). Size distributions of the FND particles before and after BSA coating were determined with a particle size and zeta-potential analyzer (Delsa Nano C, Beckman-Coulter). The final concentration of the BSA-coated FNDs in PBS was 2 mg/mL.

2.3. Animals

BALB/c male nude mice and male Sprague Dawley® (SD) rats were purchased from BioLASCO (Taiwan) and acclimated for 2–3 weeks in the animal facility of National Chiao Tung University. Eight-week old mice were used in this experiment and each mouse weighed about 20 g. Similarly, the rats were 8 weeks of age and each weighed approximately of 400–600 g at the beginning of the experiment. Both animals were housed in polycarbonate cages (maximum of 3 rats per cage) with wooden chip bedding and corn stalks. Bedding was changed twice a week. Drinking water and conventional feed were provided *ad libitum*. The animal facility has a 12-h light/dark cycle with the temperature controlled at 23 ± 1 °C and a relative humidity of 39%–43%. All the animals were maintained under specific pathogen-free conditions and were treated benevolently to eliminate or reduce suffering during the entire study, approved by the Institutional Animal Care and Use Committee of National Chiao Tung University. The complete study was conducted with compliance of standards established in the Guide for the Care and Use of Laboratory Animals.

2.4. Fodder and water uptake

Water and fodder were added twice a week. The amount of fodder consumed by rats was calculated from the difference between the weight of the ration offered and the amount removed from the feeder. Likewise, the extent of water uptake was calculated from the difference in the volume of water provided and the amount of water that was left in the bottle.

2.5. Weight changes and organ indices

Individual rats of PBS-injected (control) and FND-injected groups were weighed weekly. The mean body weights of the groups were plotted against time to reveal the course of weight gain or loss between the control and test groups. Likewise, organ indices were recorded for control and FND-treated animals. The rats were sacrificed and organs were excised and weighed. Organ indices (in g/g) were calculated from the ratios of the wet weights of the individual organs to the whole body weights (b.w.).

2.6. Subcutaneous administration

SD rats were anesthetized with isoflurane and their dorsal hair was clipped (Animal Clipper Model 900, Thrive) and a depilatory agent was applied to the skin to remove any remaining hair. FNDs were injected subcutaneously into the right flank of the rat with a dose of 0.5 mg per 500 μL PBS.

2.7. Intradermal administration

BALB/c male nude mice were initially anesthetized with isoflurane. BSA-coated FNDs were injected intradermally into the right foot paw at a dose of 40 μg in 20 μL of PBS. Similarly for the control, 20 μL BSA-PBS was injected intradermally to the left paw.

2.8. Intraperitoneal administration

FNDs were injected into SD rats via i.p. administration at a dose of 5 mg/kg b.w. Control groups of the rats were exposed to PBS solution. In order to observe the fate and long-term effect, the rats were injected every week at the same dose (5 mg/kg b.w.) continuously for 12 weeks. They were then sacrificed after 12 weeks of FND injection and their organs such as lung, liver, kidney, spleen, heart and blood were collected for organ index analysis. This group of rats was considered as the non-recovery group. In a parallel experiment, another group of rats were treated for 12 weeks with the same dosage as above and were allowed to recover for 8 weeks. This group was named as the recovery group. After the recovery period, tissue samples were cut apart and weighed for organ index analysis.

2.9. In vivo and ex vivo fluorescence imaging

Fluorescence snapshots of mice or rats were acquired after administration of FND particles by either s.c., i.d., or i.p. injection using an *in vivo* imaging system (Xenogen IVIS Spectrum, Caliper Life Sciences). Background tissue autofluorescence was first measured by photoexcitation of the living animals at the wavelength of 430 nm with a bandwidth of 35 nm. The resulting fluorescence emission was collected at 780 nm with a bandwidth of 20 nm. Sample fluorescence images were then taken by excitation at 605/20 nm and collection of the emission at 780/20 nm. The typical exposure time was 30 s. The acquired images were finally analyzed with the Living Image 4.1 software.

2.10. Histopathological examination

Dissected lymph nodes and resected tissue specimens were fixed in 10% formalin, embedded individually in paraffin blocks, and sectioned into 5 μm thickness. The sections were then stained with hematoxylin and eosin (H&E) and examined by using an Olympus BX51 light microscope.

2.11. Transmission electron microscopy

Dissected lymph nodes were fixed in 4% paraformaldehyde and 2.5% glutaraldehyde in 0.1 M cacodylate buffer (pH 7.4) for 24 h at 48 °C. After post-fixing in 1% osmium tetroxide for 1 h at room temperature, the samples were dehydrated in a gradient alcohol series, immersed in acetone, infiltrated with the increasing ratio of resin to acetone, and embedded in pure Spurr's resin (Electron Microscopy Sciences, Hatfield). Ultrathin sectioning was performed on a Leica EM UC7 ultramicrotome. The ultrathin sections (70 nm thickness) were then collected on copper grids, stained with uranyl acetate and lead citrate, and finally examined under a Hitachi 7000 electron microscope.

3. Results and discussion

3.1. In vivo stability

When a nanoparticle is introduced into the body, it is prone to enzymatic degradation or phagocytic attack. The durability of the nanoparticle as a contrast agent *in vivo* varies, depending on its composition. Recent studies have shown that porous silicon nanoparticles are biodegradable [35] whereas carbon dots of similar size are highly biostable [36]. In order to develop FND into a long-term *in vivo* contrast agent, it is important to study its stability in small animal models at high doses. The study is also crucial for its application as an advanced drug delivery device [37–42]. To address this question, we subcutaneously injected bare FND particles into a SD rat. Compared to *in vivo* imaging with the mouse model, the experiment with rats is considerably more challenging because of their greater skin thickness. The typical thickness of a rat skin is of the order of 2.0 mm, which is about 5-fold greater than that (0.45 mm) of the mouse skin. Juzenas et al. [43] have measured the wavelength dependence of light through mouse and rat skins of different thickness. They defined a penetration depth (δ) of light into the skin as the depth where the light intensity decreases to $1/e$ of the light incident on the skin surface,

and found that the penetration depth increases from $\delta = 0.6$ mm at 532 nm, $\delta = 1.7$ mm at 605 nm, to $\delta = 2.6$ mm at 780 nm. The reflectance of light from the skin surface is ~60%.

Fig. 1b shows *in vivo* fluorescence images of a rat after s.c. injection of bare FNDs (size ~ 100 nm [11]) into the right flank at a dose of 0.5 mg in 500 μL PBS. The imaging was carried out by exciting the specimens at 605/20 nm and collecting the fluorescence at 780/20 nm. The images were displayed after correction of tissue autofluorescence by subtracting the scaled background filter images (obtained at 430/35 nm excitation) from the primary filter images in order to achieve better image quality [44]. As revealed by the autofluorescence-corrected images, the fluorescence intensity of the injected FNDs stayed essentially the same over 37 days post-dosing. The weight of the rat, in contrast, is nearly doubled during the same time period of the study. It indicates that FNDs are robust *in vivo* and potentially useful as a long-term imaging agent for living animals.

3.2. Long-term biocompatibility

With the confirmation of the robustness of FNDs *in vivo*, we conducted additional imaging of the particles administrated by i.p. injection. The reason to choose this route is because the injection is simple and reproducible, and frequently generates a depot effect which allows the nanoparticles to stay in the peritoneum for several hours. It also eliminates the possibility of particle accumulation in the lung and prohibits the nanoparticles to cross the blood brain barrier [45]. Fig. 2a and b shows the results for the i.p. injection of 2 mg FNDs in 200 μL PBS for a rat starved for 1 day prior to imaging to reduce background endogenous fluorescence originating from the food in the stomach [44]. As seen, the intensity of the far-red fluorescence gradually decreases and disappears in 6 min, in stark contrast to that of the s.c. injection. The disappearance of the fluorescence signal is most likely to be a result that the injected FNDs are dispersed gradually throughout the peritoneal cavity rather than being degraded or digested in the cavity. Such a consideration is indeed supported by an *ex vivo* imaging study of the organs and tissues of the rat sacrificed on day 8, where most of the FND particles are found on the surface of mesentery and serosa of the stomach (Fig. 2c). In comparison, the parenchyma of the abdominal organs is almost free of FND particles.

Next, we performed experiments to study the long-term biocompatibility of the particles after i.p. injection. Specifically, we studied the sub-acute toxicity of the intraperitoneally administered FNDs over a time period of 5 months. In this experiment, the rats were injected weekly at a dose of 5 mg/kg b.w. continuously for 12 weeks. One half of the group (*i.e.* the non-recovery group) of the rats was sacrificed after 12 weeks of FND injection and another half group (*i.e.* the recovery group) was allowed to recover for 8 weeks without any injection. Measurements of water consumption, fodder consumption, and body weight of the rats were conducted every week. The results are displayed in Fig. 3 and Figure S3 showing no significant differences between control (PBS-treated) and FND-treated recovery/non-recovery groups. In addition to these physiological parameters, organ indices, which provide information on the general toxicity, were also measured at the end of this experiment. The organ index is defined as the ratio of the wet weight of the organ (g) to the whole body weight (g), and increases or decreases of the indices denote added or reduced function of the individual organs [15]. Shown in Fig. 4 is a typical set

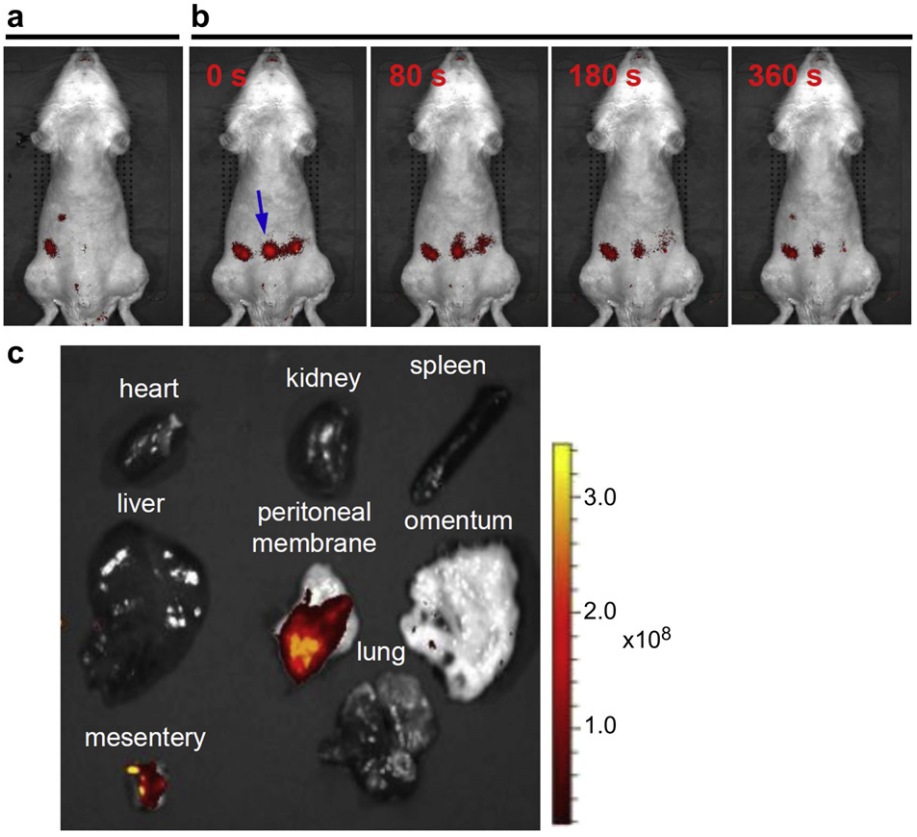

Fig. 2. *In vivo* and *ex vivo* imaging of FNDs in a rat after i.p. injection. (a, b) *In vivo* images acquired before injection (a) and at 0, 80, 180, and 360 s after injection (b), showing rapid spread of the FND particles in the peritoneal cavity. Blue arrow indicates the site of injection. (c) *Ex vivo* images of the extracted tissues and organs. (For interpretation of the references to color in this figure legend, the reader is referred to the web version of this article.)

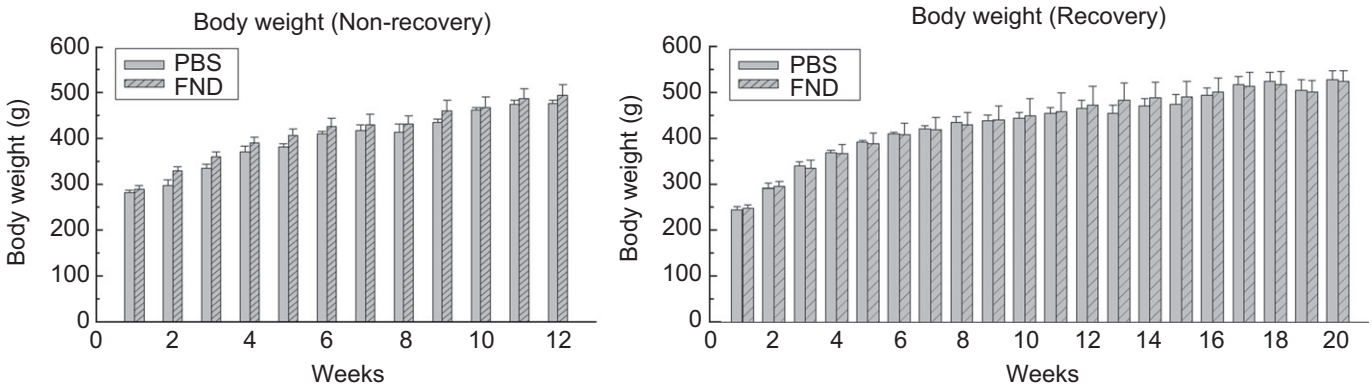

Fig. 3. Comparison of the body weights of PBS-injected (control) and FND-injected SD rats (with a dose of 5 mg/kg b.w. per week) over a time period of 3 and 5 months for the non-recovery and recovery groups ($n = 3$ each), respectively. The injection was carried out by i.p. administration.

of data for the measurement. Again, there is no significant difference in the organ indices of control and FND-injected rats for both the recovery and non-recovery groups, indicating that multiple injections of the bare FNDs do not cause obvious toxicological effects. Taken together, these results corroborate the suggestion that the FND administration does not induce any apparent toxicity in rats during the study period of 5 months. Furthermore, no abnormal clinical signs or behaviors were detected in either control or FND-injected animals during the entire course of the study.

To provide more direct information on the existence of FNDs in the animals, we acquired dissection images of the rats after i.p. injection of FNDs for 8 weeks. As displayed in Figure S4, the FNDs in the non-recovery group tend to accumulate initially on mesentery and serous membrane of the stomach, similar to the finding of Fig. 2c. Digestion of the membrane in concentrated nitric acid and subsequent fluorescence spectroscopic measurement (procedures detailed in Figure S5 along with the fluorescence spectrum displayed in Figure S6) confirmed that the white patches seen on the serous membrane are FNDs. In comparison, the recovery group of the FND-injected rats showed much less accumulation of FNDs in the stomach serous membrane. It suggests that FNDs have been either absorbed or transported from the site of injection to other regions of the mouse body after 8 weeks of recovery.

In order to find out whether the injected FNDs will cause any damage *in vivo*, detailed histological examination of all tissue sections was carried out. Microscopically, no significant difference was seen between the FND-treated and control groups (Fig. 5a) except that carbon-laden macrophages (*i.e.* the dark brown color spots) cluster on the peritoneal surface of the FND-treated animals but not in the control group (Fig. 5b). Comparing the optical micrographs of these two groups strongly indicates that the carbon particles within these macrophages are engulfed FND particles. We do not observe any inflammation, necrosis, or tissue reaction surrounding these carbon-laden macrophages. Moreover, no FNDs or other specific pathological changes could be identified in the wall of gastrointestinal tract or parenchyma of visceral organs, such as liver, spleen, kidney, heart and lung in the treated animals. All the examinations confirm the long-term biocompatibility of FNDs. The excellent biocompatibility of the sp^3-carbon-based nanomaterial makes it superior to other nanoparticles, such as nanosilica which has very recently been reported to cause liver injury after continuous intraperitoneal injection [46], for *in vivo* applications.

3.3. Sentinel lymph node imaging

Sentinel lymph node mapping is one of the most important and routine procedures in cancer treatment. SLNs are the group of lymph nodes which receive the metastasizing cancer cells from the primary tumor [47]. Thus, the status of SLNs (such as the axillary lymph nodes, ALNs) is a critical factor in predicting

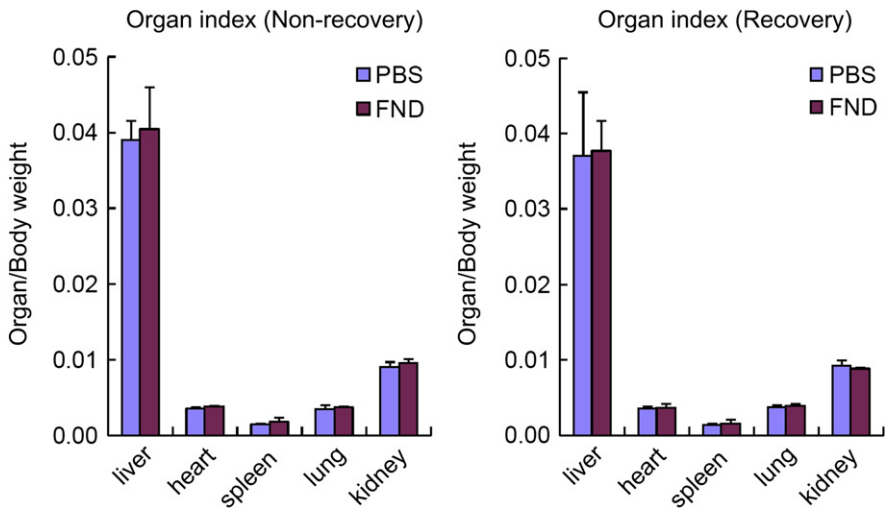

Fig. 4. Comparison of the organ indices of PBS-injected (control) and FND-injected SD rats (with a dose of 5 mg/kg b.w. per week) after 12 weeks of treatment for the non-recovery and recovery groups ($n = 3$ each), respectively. The injection was carried out by i.p. administration.

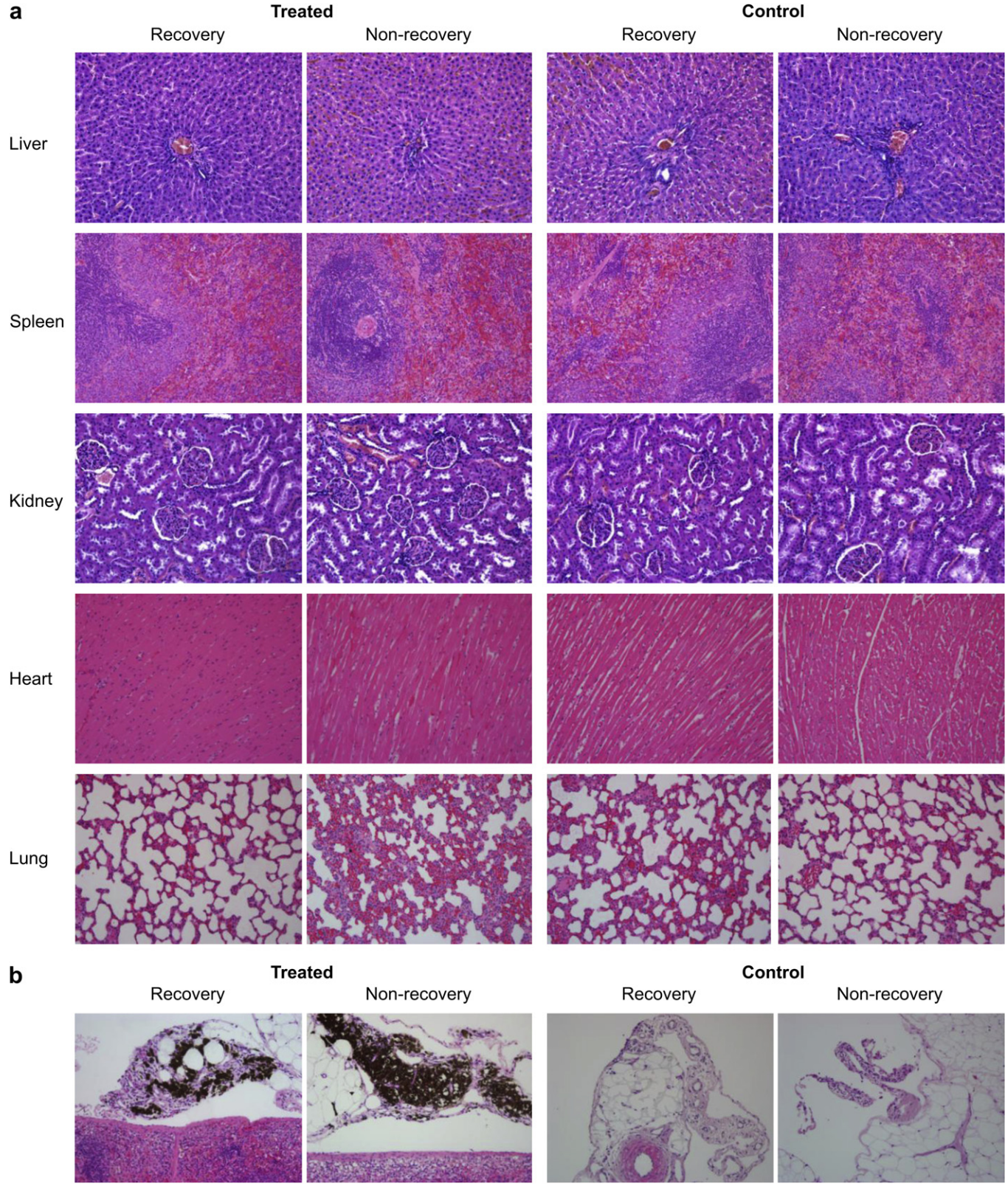

Fig. 5. Histopathological examination of the tissue sections of FND-injected (treated) and PBS-injected (control) SD rats with and without recovery. (a) Images showing no specific pathological changes in both FND-treated and control groups (magnification 200×). (b) Images showing clustering of carbon-laden macrophages (appearing as dark brownish spots) on the peritoneal surface of the spleen in the FND-injected rats but not in the BSA-injected rats (magnification 200×). (For interpretation of the references to color in this figure legend, the reader is referred to the web version of this article.)

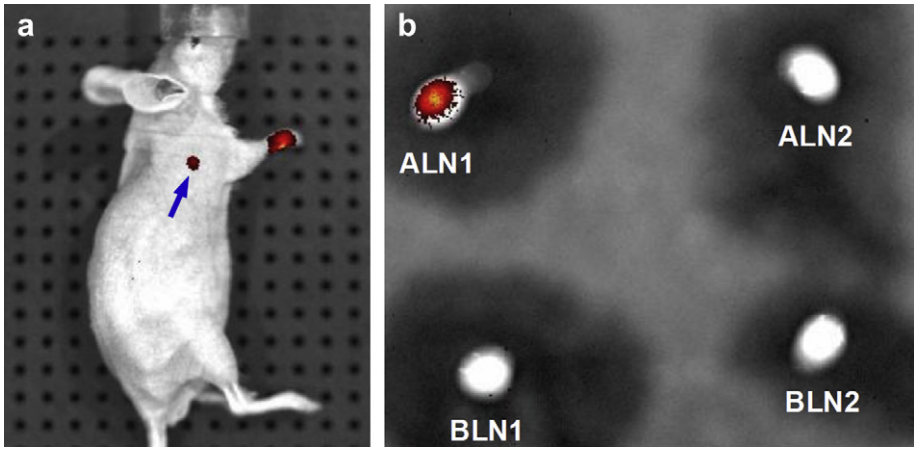

Fig. 6. *In vivo* and *ex vivo* lymph node imaging of a nude mouse after i.d. injection of BSA-coated FNDs. (a) *In vivo* image showing accumulation of the FND particles in the right axillary lymph node (indicated by the blue arrow) on day 8. Note that most of the injected FND particles remain trapped at the injection site. (b) *Ex vivo* fluorescence image of four extracted lymph nodes, where ALN1 and ALN2 are the lymph nodes located at the right and left axilla, respectively, and BLN1 and BLN2 are the lymph nodes located at the right and left brachial regions, respectively. (For interpretation of the references to color in this figure legend, the reader is referred to the web version of this article.)

prognosis of the patients as well as the determination of further treatment [48]. Traditional SLN imaging with radioisotopes and blue dye is well established in clinical applications, but recent researches show that nanoparticles with size in the range of 1–100 nm are also applicable for lymph node mapping [49]. To explore the possibility of using FNDs for this application, nude mice were injected intradermally with 100-nm FNDs coated noncovalently with BSA. The coating was made to facilitate the dispersibility of the particles in PBS as well as in biological medium [34]. The BSA-coated FND particles were then injected into the right foot paw of a mouse at a dose of 40 μg in 20 μL of PBS. Fig. 6a shows an autofluorescence-corrected image acquired on day 8, where the intradermally injected FNDs can be clearly detected not only at the injection site, but also at the ALN closest to the right foot paw. To further confirm that the observed bright red spot (indicated by a blue arrow) is indeed associated with SLN, the mouse was sacrificed on day 8 and four major lymph nodes were dissected out for fluorescence imaging *ex vivo* (Fig. 6b). In accord with the finding of *in vivo* imaging, the FNDs are predominantly accumulated at the lymph node ALN1 located at the right axilla of the mouse [50]. No FNDs were detected in the left axillary lymph node (ALN2) and in the brachial lymph nodes (BLN1 and BLN2) within the sensitivity limit of our fluorescence measurements. The observations are consistent with a mechanism that most of the intradermally administered FNDs are accumulated in the dermis and engulfed by the macrophages. The remaining particles are collected by the dermal lymphatics and drained into the lymphatic channels of the upper limb. As the lymphatic channels of the upper extremity converge to the ALN of the same side, the nanoparticles within the lymphatic channels are therefore preferentially collected by the lymph node that first receives the drainage (*i.e.* the ALN1).

Fig. 7 presents the result of a histopathological examination for the skin of a mouse right paw where BSA-coated FNDs were intradermally injected. Indeed, it is found that the majority of the FND-containing macrophages (*i.e.* the dark brown color spots) aggregate in the dermis of the skin close to the skeletal muscle. No inflammation or reaction of any kind to the injected FND particles was observed. To further examine if the accumulation of the BSA-coated FNDs in SLNs can lead to any significant damage or changes, histological analysis and transmission electron microscopy imaging of the resected lymph nodes were performed. Histologically, clustering of carbon-laden cells is present in the paracortex of the ALN1 without other noticeable pathological changes (Fig. 8). Ultrastructurally, these carbon particles appear refractile and electron-dense, which is compatible with the characteristics of FND nanocrystallites (Fig. 9). Additionally, these nanoparticles are located in the cytoplasm of the macrophages, which are characterized by the presence of abundant lysosomes and vacuoles in their cytoplasm.

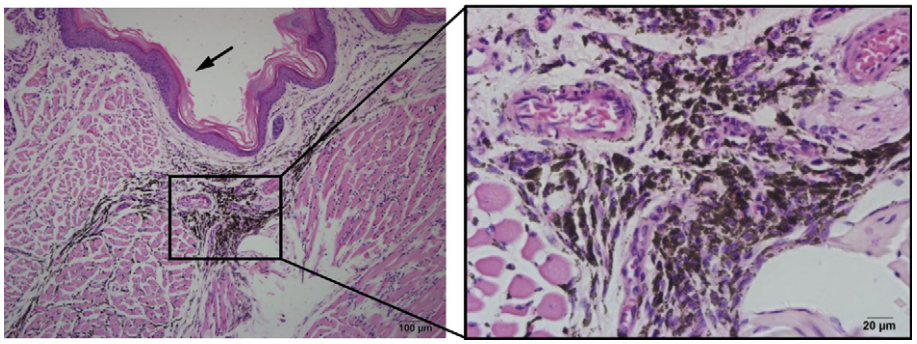

Fig. 7. Histological examination of the skin of an FND-treated mouse by H&E staining. The black arrow indicates the epidermis (magnification 100×). Macrophages, appearing as dark brownish carbon-laden cells, are found to cluster in the dermis of the right paw, where BSA-coated FNDs were injected. No inflammation, necrosis, or tissue damage occurred in the surrounding cells. (For interpretation of the references to color in this figure legend, the reader is referred to the web version of this article.)

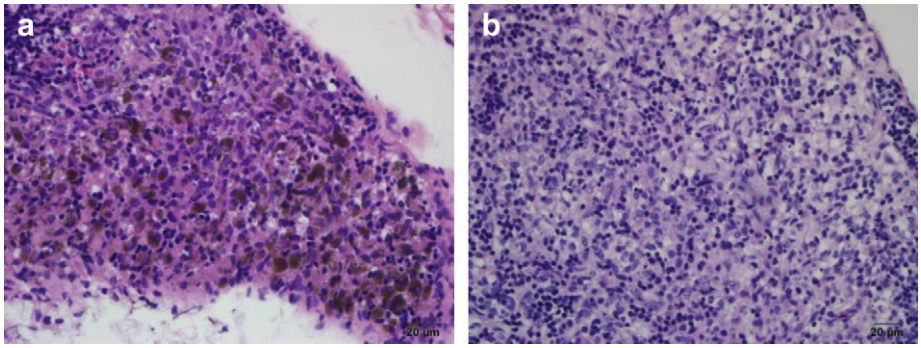

Fig. 8. H&E-stained sections of the lymph nodes, (a) ALN1 and (b) ALN2, of a BSA-FND-treated mouse. ALN1 and ALN2 are the axillary lymph nodes dissected from the injected and non-injected sides of the mouse body, respectively. Brownish carbon-laden macrophages are seen to gather in the paracortical zone of the ALN1 lymph node but not in that of ALN2 (magnification 400×). (For interpretation of the references to color in this figure legend, the reader is referred to the web version of this article.)

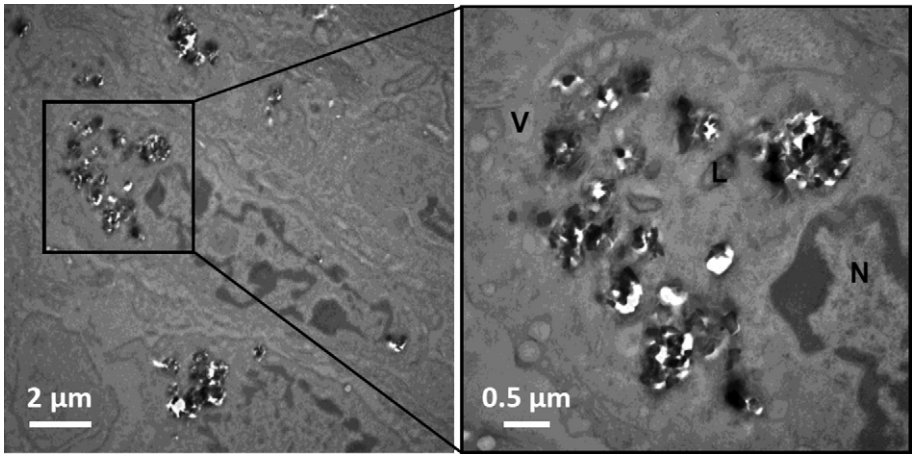

Fig. 9. Electron microscopic examination of carbon-laden cells in the ALN1 lymph node of a BSA-FND-treated mouse after i.d. injection. Refractile and electron-dense FND particles are found in the cytoplasm of the lymph node cells. These cells have many lysosomes and vacuoles in their cytoplasm (L: lysosome, N: nucleus, V: vacuole), which are characteristic of macrophages.

4. Conclusion

This work demonstrates that diamond nanoparticles containing built-in NV^- fluorophores can be used as an *in vivo* contrast agent for small animal models like mice and rats. The high stability of the FND particles under physiological conditions makes it possible to observe their fluorescence emission over 37 days after injection by either subcutaneous or intraperitoneal administration. Moreover, the drainage of the 100-nm FND particles from the intradermal injection site to SLN is readily detectable both *ex vivo* and *in vivo* by using a standard imaging system. Further improvement of the image contrast is feasible by utilizing the long fluorescence lifetime and the magneto-optical property of the NV^- centers with more advanced imaging schemes. The effective SLN mapping with FNDs, as illustrated herein, paves the way for the development a nanodiamond-based real-time optical guidance method, by which surgeons can precisely identify superficial SLNs non-invasively or reveal deep SLNs by tracing the fluorescently visualized lymphatics during surgery. We believe that FND is worthy of further optimization of performance as well as toxicity evaluations for clinical translation.

Acknowledgments

This work is supported by Academia Sinica and the National Science Council (NSC) of Taiwan with Grant Nos. NSC 100-2119M-001-028 and NSC 99-2311-B-009-003-MY3. We thank the Taiwan Mouse Clinic, funded by the National Research Program for Genomic Medicine (NRPGM) at NSC for technical support in tissue sectioning. We also thank Wan-Yu Hsieh at the National Taiwan University and Tzu-Han Hsu at the Core Facility of the Institute of Cellular and Organismic Biology, Academia Sinica, for assistance in fluorescence and TEM imaging.

Appendix A. Supplementary material

Supplementary material related to this article can be found online at http://dx.doi.org/10.1016/j.biomaterials.2012.06.084.

References

[1] Service RF. Nanotechnology takes aim at cancer. Science 2005;310:1132–4.
[2] Peer D, Karp JM, Hong S, Farokhzad OC, Margalit R, Langer R. Nanocarriers as an emerging platform for cancer therapy. Nat Nanotechnol 2007;2:751–60.
[3] Sanhai WR, Sakamoto JH, Canady R, Ferrari M. Seven challenges for nanomedicine. Nat Nanotechnol 2008;3:242–4.
[4] Vaijayanthimala V, Chang HC. Functionalized fluorescent nanodiamonds for biomedical applications. Nanomedicine 2009;4:47–55.
[5] Xing Y, Dai L. Nanodiamonds for nanomedicine. Nanomedicine 2009;4:207–18.
[6] Ho D, editor. Nanodiamonds: applications in biology and nanoscale medicine. Morwell: Springer; 2009.
[7] Mochalin VN, Shenderova O, Ho D, Gogotsi Y. The properties and applications of nanodiamonds. Nat Nanotechnol 2012;7:11–23.
[8] Schrand AM, Johnson J, Dai L, Hussain SM, Schlager JJ, Zhu L, et al. Cytotoxicity and genotoxicity of carbon nanomaterials. In: Webster TJ, editor. Safety of

nanoparticles, nanostructure science and technology. Morwell: Springer; 2009. p. 159–87.
[9] Xing Y, Xiong W, Zhu L, Osawa E, Hussin S, Dai L. DNA damage in embryonic stem cells caused by nanodiamonds. ACS Nano 2011;5:2376–84.
[10] Liu KK, Wang CC, Cheng CL, Chao JI. Endocytic carboxylated nanodiamond for the labelling and tracking of cell division and differentiation in cancer and stem cells. Biomaterials 2009;30:4249–59.
[11] Fang CY, Vaijayanthimala V, Cheng CA, Yeh SH, Chang CF, Li CL, et al. The exocytosis of fluorescent nanodiamond and its use as a long-term cell tracker. Small 2011;7:3363–70.
[12] Zaitsev AM. Optical properties of diamond: a data handbook. Morwell: Springer; 2010.
[13] Puzyr AP, Baron AV, Purtov KV, Bortnikov EV, Skobelev NN, Mogilnaya OA, et al. Nanodiamonds with novel properties: a biological study. Diam Relat Mater 2007;16:2124–8.
[14] Yuan Y, Chen Y, Liu JH, Wang H, Liu Y. Biodistribution and fate of nanodiamonds *in vivo*. Diam Relat Mater 2009;18:95–100.
[15] Yuan Y, Wang X, Jia G, Liu JH, Wang T, Gu Y, et al. Pulmonary toxicity and translocation of nanodiamonds in mice. Diam Relat Mater 2010;19:291–9.
[16] Marcon L, Riquet F, Vicogne D, Szunerits S, Bodart JF, Boukherroub R. Cellular and *in vivo* toxicity of functionalized nanodiamond in Xenopus embryos. J Mater Chem 2010;20:8064–9.
[17] Rojas S, Gispert JD, Martin R, Abad S, Menchón C, Pareto D, et al. Biodistribution of amino-functionalized diamond nanoparticles. In vivo studies based on ^{18}F radionuclide emission. ACS Nano 2011;5:5552–9.
[18] Mohan N, Chen CS, Hsieh HH, Wu YC, Chang HC. *In vivo* imaging and toxicity assessments of fluorescent nanodiamonds in *Caenorhabditis elegans*. Nano Lett 2010;10:3692–9.
[19] Mohan N, Zhang B, Chang CC, Yang L, Chen CS, Fang, CY, et al. Fluorescent nanodiamond – a novel nanomaterial for in vivo applications. MRS Proceedings 2011;1362:mrss11-1362-qq06-01.
[20] Bonnema J, van de Velde CJH. Sentinel lymph node biopsy in breast cancer. Ann Oncol 2002;13:1531–7.
[21] Kim S, Lim YT, Soltesz EG, DeGrand AM, Lee J, Nakayama A, et al. Near-infrared fluorescent type II quantum dots for sentinel lymph node mapping. Nat Biotechnol 2004;22:93–7.
[22] Pons T, Pic E, Lequeux N, Cassette E, Bezdetnaya L, Guillemin F, et al. Cadmium-free CuInS2/ZnS quantum dots for sentinel lymph node imaging with reduced toxicity. ACS Nano 2010;4:2531–8.
[23] Yu SJ, Kang MW, Chang HC, Chen KM, Yu YC. Bright fluorescent nanodiamonds: no photobleaching and low cytotoxicity. J Am Chem Soc 2005;127:17604–5.
[24] Fu CC, Lee HY, Chen K, Lim TS, Wu HY, Lin PK, et al. Characterization and application of single fluorescent nanodiamonds as cellular biomarkers. Proc Natl Acad Sci U S A 2007;104:727–32.
[25] Chang YR, Lee HY, Chen K, Chang CC, Tsai DS, Fu CC, et al. Mass production and dynamic imaging of fluorescent nanodiamonds. Nat Nanotechnol 2008;3:284–8.
[26] Davies G. Vibronic spectra in diamond. J Phys C Solid State Phys 1974;7:3797–809.
[27] Weissleder R, Ntziachristos V. Shedding light onto live molecular targets. Nat Med 2003;9:123–8.
[28] Hui YY, Cheng CL, Chang HC. Nanodiamonds for optical bioimaging. J Phys D Appl Phys 2010;43:374021.
[29] Collins AT, Thomaz MF, Jorge MIB. Luminescence decay time of the 1.945 eV center in type Ib diamond. J Phys C Solid State 1983;16:2177–81.
[30] Urayama PK, Mycek MA. Fluorescence lifetime imaging microscopy of endogenous biological fluorescence. In: Mycek MA, Pogue BW, editors. Handbook of biomedical fluorescence. New York: Marcel Dekker; 2003. p. 211–6.
[31] Chang CW, Sud D, Mycek MA. Fluorescence lifetime imaging microscopy. Methods Cell Biol 2007;81:495–524.
[32] Faklaris O, Garrot D, Joshi V, Druon F, Boudou JP, Sauvage T, et al. Detection of single photoluminescent diamond nanoparticles in cells and study of the internalization pathway. Small 2008;4:2236–9.
[33] McGuinness LP, Yan Y, Stacey A, Simpson DA, Hall LT, Maclaurin D, et al. Quantum measurement and orientation tracking of fluorescent nanodiamonds inside living cells. Nat Nanotechnol 2011;6:358–63.
[34] Tzeng YK, Faklaris O, Chang BM, Kuo Y, Hsu JH, Chang HC. Superresolution imaging of albumin-conjugated fluorescent nanodiamonds in cells by stimulated emission depletion. Angew Chem Int Ed 2011;50:2262–5.
[35] Park JH, Gu L, von Maltzahn G, Ruoslahti E, Bhatia SN, Sailor MJ. Biodegradable luminescent porous silicon nanoparticles for *in vivo* applications. Nat Mater 2009;8:331–6.
[36] Yang ST, Cao L, Luo PG, Lu F, Wang X, Wang HF, et al. Carbon dots for optical imaging *in vivo*. J Am Chem Soc 2009;131:11308–9.
[37] Huang H, Pierstorff E, Osawa E, Ho D. Active nanodiamond hydrogels for chemotherapeutic delivery. Nano Lett 2007;7:3305–14.
[38] Liu KK, Chen MF, Chen PY, Lee TJF, Cheng CL, Chang CC, et al. Alpha-bungarotoxin binding to target cell in a developing visual system by carboxylated nanodiamond. Nanotechnology 2008;19:205102.
[39] Guan B, Zou F, Zhi JF. Nanodiamond as the pH-responsive vehicle for an anticancer drug. Small 2010;6:1514–9.
[40] Liu KK, Zheng WW, Wang CC, Chiu YC, Cheng CL, Lo YS, et al. Covalent linkage of nanodiamond-paclitaxel for drug delivery and cancer therapy. Nanotechnology 2010;21:315106.
[41] Li XX, Shao JQ, Qin Y, Shao C, Zheng TT, Ye L. TAT-conjugated nanodiamond for the enhanced delivery of doxorubicin. J Mater Chem 2011;21:7966–73.
[42] Chow EK, Zhang XQ, Chen M, Lam R, Robinson E, Huang HJ, et al. Nanodiamond therapeutic delivery agents mediate enhanced chemoresistant tumor treatment. Sci Transl Med 2011;3:73ra21.
[43] Juzenas P, Juzeniene A, Kaalhus O, Iani V, Moan J. Noninvasive fluorescence excitation spectroscopy during application of 5-aminolevulinic acid *in vivo*. Photochem Photobiol Sci 2002;1:745–8.
[44] Troy T, Jekic-McMullen D, Sambucetti L, Rice B. Quantitative comparison of the sensitivity of detection of fluorescent and bioluminescent reporters in animal models. Mol Imag 2004;3:9–23.
[45] Intra J, Salem AK. Characterization of the transgene expression generated by branched and linear polyethylenimine-plasmid DNA nanoparticles *in vitro* and after intraperitoneal injection *in vivo*. J Control Release 2008;130:129–38.
[46] Liu T, Li L, Fu C, Liu H, Chen D, Tang F. Pathological mechanisms of liver injury caused by continuous intraperitoneal injection of silica nanoparticles. Biomaterials 2012;33:2399–407.
[47] Jakub JW, Pendas S, Reintgen DS. Current status of sentinel lymph node mapping and biopsy: facts and controversies. Oncologist 2003;8:59–68.
[48] Robe A, Pic E, Lassalle HP, Bezdetnaya L, Guillemin F, Marchal F. Quantum dots in axillary lymph node mapping: biodistribution study in healthy mice. BMC Cancer 2008;8.
[49] Moghimi SM, Hunter AC, Murray JC. Nanomedicine: current status and future prospects. Faseb J 2005;19:311–30.
[50] Jeon YH, Kim YH, Choi K, Piao JY, Quan B, Lee YS, et al. *In vivo* imaging of sentinel nodes using fluorescent silica nanoparticles in living mice. Mol Imag Biol 2010;12:155–62.